ORIGINAL ARTICLE
DOI: 10.5433/1679-0375.2022v43n1p21

Modified sol-gel synthesis of lithium ternary oxide $LiNi_{1/3}Mn_{1/3}Co_{1/3}O_2$ for lithium-ion rechargeable batteries

Síntese sol-gel modificada de óxido ternário litiado $LiNi_{1/3}Mn_{1/3}Co_{1/3}O_2$ para baterias recarregáveis de íon-lítio

Maria Gabriella Detone Guaita[1]; Luiz Henrique Dall'Antonia[2];
Paulo Rogério Catarini da Silva[3]; Alexandre Urbano[4]

Abstract

Lithium-ion batteries currently equip portable electronic devices, such as smartphones and laptops, and are the choice to power electric vehicles. The scarcity of raw materials in nature, however, has required the development of new technologies and the ternary lithium compound $LiNi_{1/3}Mn_{1/3}Co_{1/3}O_2$ has stood out as an alternative for replacing part of the cobalt in $LiCoO_2$ by nickel and manganese, which are more abundant, reducing the electrode's cost. The sol-gel route for synthesis of ternary electrode materials has been widely used, but it faces problems of volumetric expansion due to the decomposition of organic material during calcination. To improve the synthesis of the ternary compound, a modified sol-gel route with control of the heating kinetics in the pre-calcination step and without pH control was investigated in this study. The compound was analyzed by X-ray diffraction, Rietveld refinement, Fourier transform infrared absorption spectroscopy, and Raman that showed the purification of the ternary phase with appropriate crystallinity for application as electrode in batteries from 700 ºC. In conclusion, ternary synthesis with rate control during heat treatment may be a useful alternative for industrial scale-up production.

Keywords: Sol-gel; lithium-ion batteries; synthesis; size-strain.

Resumo

Baterias recarregáveis de íon-lítio equipam atualmente dispositivos eletrônicos portáteis e prometem abastecer de energia elétrica veículos automotores num futuro próximo. A escassez de matéria prima na natureza, contudo, tem exigido o desenvolvimento de novas tecnologias e o composto litiado ternário $LiNi_{1/3}Mn_{1/3}Co_{1/3}O_2$ tem se destacado como alternativa por substituir parte do cobalto por níquel e manganês, que são mais abundantes, barateando o eletrodo. A rota sol-gel para síntese do eletrodo ternário tem sido utilizada, mas enfrenta problemas de expansão volumétrica devido à decomposição do material orgânico durante a calcinação. Para aprimorar a síntese do composto ternário, investigou-se nesse trabalho uma rota sol-gel modificada com controle da cinética de aquecimento na etapa de pré-calcinação e sem controle de pH. O composto foi analisado por DRX, refinamento de Rietveld, FTIR e Raman que mostraram que a purificação da fase de ternário com cristalinidade apropriada para aplicação como eletrodo em baterias acontece a partir de 700 ºC. Em conclusão a síntese do ternário, com controle da taxa de aquecimento no tratamento térmico, pode ser uma alternativa útil para aplicação em escala industrial.

Palavras-chave: Sol-gel; baterias de íon-lítio; síntese; size-strain.

[1] MSc., Department of Chemistry, UEL, Londrina, Paraná, Brazil, E-mail: gabriellaguaita@hotmail.com
[2] Prof. Dr., Department of Chemistry, UEL, Londrina, Paraná, Brazil, E-mail: luizh@uel.br
[3] Prof. Dr., Department of Physic, UEL, Londrina, Paraná, Brazil, E-mail: prcsilva@uel.br
[4] Prof. Dr., Department of Physic, UEL, Londrina, Paraná, Brazil, E-mail: aurbano@uel.br

Introduction

Lithium-ion batteries dominate the wireless device market, and more recently, since the 2000s, the demand for electric vehicle applications has been increasing (WANG *et al*., 2022). There are billions of units produced to feed both markets and consequently major impact on nature reserves mainly for lithium and cobalt elements. These elements, besides being scarce, are poorly distributed throughout the planet (VAALMA *et al*., 2018). One alternative to partially replace cobalt in these batteries is the use of $LiNi_{1/3}Mn_{1/3}Co_{1/3}O_2$ in place of $LiCoO_2$ cathode material, which in addition to reducing the amount of cobalt can increase energy density at a lower cost (CAO *et al.*, 2016; WANG *et al*., 2022).

The $LiNi_{1/3}Mn_{1/3}Co_{1/3}O_2$ (NMC), first synthesized in 2001 by Ohzuku and Makimura (2001), has a high specific capacity (200 mA h g^{-1} in the 2.80 to 4.60 V potential window), lower cost and toxicity, due to the low content of cobalt, and higher thermal stability compared to $LiCoO_2$. NMC can be described as a solid solution between $LiNiO_2$, $LiMnO_2$, and $LiCoO_2$, combining high nickel-associated capacity and long-life cycle, the safety of manganese compound, and high cobalt-related electronic conductivity and structural stability.

Similarly, the NMC has a lamellar structure made up of lithium-ion intercalated into the transition metal oxide (MO_6) layers (CAO *et al.*, 2016; JAMIL *et al.*, 2009; SATHIYA *et al*., 2009).

The atomic structure and morphology of lithium transition metal oxides substantially affect the electrochemical performance of these electrode compounds. NMC is generally synthesized by routes that require high temperatures to achieve a well-ordered layered structure with few crystallographic defects (SATHIYA *et al*., 2009). Position shifting between lithium and nickel ions, which leads to decreased material charge capacity, and layer stacking distortions, are the main types of defects found in NMC (CAO *et al.*, 2016; HOANG; JOHANNES, 2016; SATHIYA *et al*., 2009). While structural ordering occurs at elevated temperatures, there is also a grain growth, modifying the compound morphology.

As the synthesis method defines atomic structure and morphology, establishing the correlation between synthesis parameters and electrochemical properties becomes vital for obtaining compounds with excellent performance (SATHIYA *et al*., 2009; WANG *et al*., 2022).

Sol-gel synthesis allows for homogeneous incorporation of reagents at the molecular level, regular chemical composition and the formation of nanometric particles, which increase the surface area and intercalation efficiency of lithium ions. However, this method requires strict pH control and causes a violent volumetric expansion of the material during its calcination due to the gas released during the burning of the complexing agent, resulting in difficulties in the industrial scaling of this method (CAO *et al.*, 2016; KIZILTAŞ-YAVUZ *et al.*, 2013).

This work aimed to synthesize $LiNi_{1/3}Mn_{1/3}Co_{1/3}O_2$ compound by simplified sol-gel route, without pH adjustment and under low heating rate, in order to simplify the method and suppress volumetric expansion, evaluating its crystallographic, morphological, spectroscopic and electrochemical properties.

Materials and methods

An aqueous solution containing $LiCH_3COO.2H_2O$ (Aldrich), $Ni(CH_3COO)_2.4H_2O$ (Dynamic), $Co(CH_3CO)_2.4H_2O$ (Synth) and $Mn(CH_3COO)_2.4H_2O$ (Dynamic) was mixed with a saturated citric acid solution (Synth) at 80 ºC in a 1:1 (v/v) ratio. The obtained solution was left under stirring and heating at 80 ºC to give a pink gel. The resulting gel was pre-calcined in the air for 6 hours at 450 ºC at a heating rate of approximately 5 ºC/min. The material obtained was ground and divided into six parts; each part was then calcined in air for 1 hour at different temperatures: 550, 650, 700, 750, 800 and 850 ºC.

The crystalline structure of the samples was characterized by X-ray diffraction (XRD) in a PANanalytical diffractometer X´Pert PRO MPD model, using Bragg-Brentano geometry, with Cu kα radiation in the 10 to 90º angle range, with 0.05º angular step and 5 seconds for step time. High Score Plus software version 3.0d was used to apply the Rietveld structure refinement method. The crystallite size of all samples was determined by refining the diffractograms, equation (1), and also by applying the Scherrer equations, equation (2), and Williamson-Hall, equation (3), given by:

$$D = \left(\frac{180}{\pi}\right)\frac{\lambda}{\sqrt{W_i - W_{std}}}, \quad (1)$$

$$D = \frac{K\,\lambda}{\beta\,\cos\theta}, \quad (2)$$

$$\beta\,\cos\theta = \frac{K\,\lambda}{D} + 4\,\varepsilon\,\mathrm{sen}\theta. \quad (3)$$

In the equations (1)-(3), D corresponds to the crystallite size, W_i is the W parameter of the diffractogram refinement of the sample, W_{std} is the W parameter of the diffractogram refinement of a silicon standard, K a constant dependent on the material's grain geometry, K = 0.9 for spherical grains, λ the wavelength of the radiation, λ of Cu $K_\alpha = 0.15406$ nm, θ the peak angle (in radians) and β the width at half height of the peak (in radians). The value of β is obtained through equation (4),

$$\beta = \sqrt{\beta_{exp}^2 - \beta_{inst}^2}, \quad (4)$$

which takes into account the width at half height of the peak, taken as a Gaussian curve, of a pattern, in this case a silicon pattern, which provides a characteristic value of the instrument, β_{inst}, must be discounted from the width at half height of the peak of the experimental diffractogram, β_{exp} (BORCHERT *et al*., 2005; GONÇALVES *et al*, 2012).

The mechanical micro-strain values (ε) of all samples were obtained through refinement, equation (5),

$$\varepsilon = \frac{\sqrt{(U_i - U_{std}) - (W_i - W_{std})}}{\frac{1}{100}\left(\frac{180}{\pi}\right)4\sqrt{2\ln 2}}, \quad (5)$$

and the Williamson-Hall equation, equation (3).

In equation (5), U_i is the U parameter of the diffractogram refinement of the sample and U_{std} is the U parameter of the diffractogram refinement of a silicon standard.

Morphological analyses were performed using a Philips - FEI Quanta 200 scanning electron microscope (beam energy data, 30 kV). Chemical characterization was performed by Raman spectroscopy on the confocal InVia Raman microscopectrometer (Renishaw) with 633 nm wavelength laser and Fourier transform infrared absorption spectroscopy (FTIR) in the mid-infrared region (400-4000 cm^{-1}) on the Shimadzu 8300 (PADCT) spectrometer.

The samples calcined at 700 and 850 ºC were electrochemically characterized in a home-made button cell, with lithium metal as reference and counter electrodes. The cathode slurry consisted of 80 wt.% of the synthesized sample, 10 wt.% of poly(vinylidene difluoride) (PVDF, Sigma-Aldrich) as binder and 10 wt.% of Carbon Black (Grafite do Brasil) as an electronic conductor agent dissolved in N-methyl pyrrolidone (NMP, Synth) and deposited on an aluminum foil. After casting and drying, discs (ø 11 mm) electrodes were dried at 100 °C for 15 hours in a vacuum oven and then stored in an argon atmosphere, free of H_2O, O_2, and CO_2.

The electrodes were separated by glass fiber separator (Whatman) embedded in the 1 mol L^{-1} $LiClO_4$ solution (Sigma-Aldrich) in ethylene carbonate (Sigma-Aldrich) and dimethyl carbonate (Sigma-Aldrich) in a 1:1 (v/v) ratio as electrolyte. The electrochemical properties were analyzed through galvanostatic charge and discharge cycles at a potential range of 3.00 to 4.20 V vs. Li/Li^+ with an electric current of 0.1C (C = 124.6 mA h g^{-1}) and 0.2C. In addition, the electrodes were also cycled at 0.1C constant current at a potential of 3.00 to 4.70 V. The electrodes were cycled from 3.00 V to each of the following potentials: 4.20, 4.30, 4.40, 4.50, 4.60 and 4.70 V. The effect of the rate was examined by cycling at 0.1C, 0.2C, 1C, 2C and 5C at the potential from 3.00 to 4.70 V.

Results and discussion

X-ray diffraction

The purity and high crystallinity of layered transition metal oxides are required to obtain cathodic materials with excellent electrochemical properties.

Figure 1 shows the diffractograms of the pre-calcined (450 °C) and other calcined samples at different temperatures (550, 650, 700, 750, 800 and 850 °C). The percent weight (wt.%) quantifications of the phases identified by the Rietveld refinement are presented in Table 1.

Figure 1 – X-Ray diffractions for calcined samples.

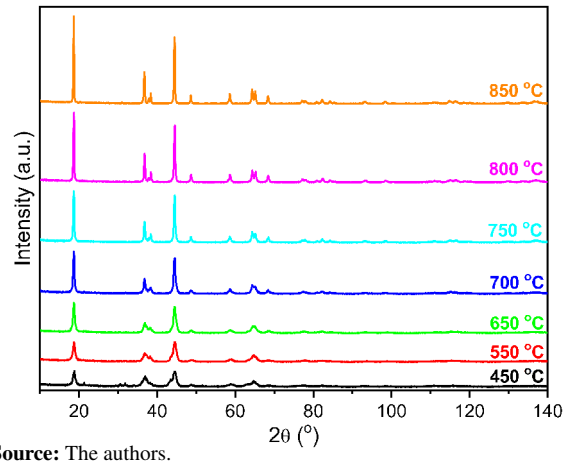

Source: The authors.

At lower temperatures a ternary (NMC), NiO, Co_3O_4 and Li_2CO_3 phases are present. Oxidation reactions occur during synthesis which allows CO_2^+ and Mn^{2+}, from acetates used as reagents, to oxidize to Co^{2+} and Mn^{4+}, respectively, to form $LiNi^{2+}{}_{1/3}Mn^{4+}{}_{1/3}Co^{3+}{}_{1/3}O_2$, as described in the literature (CHO *et al.*, 2005).

Table 1 – Rietveld refinement results for calcined samples, where NMC refers to $Li_xNi_yMn_zCo_wO_2$.

Temperature	Phases (%)					NMC Lattice Parameters			GOF
(ºC)	NMC	NiO	$Co3O_4$	Li2CO3	Ni	a (Å)	c (Å)	c/a	
450	59.5	13.5	12.2	12.9	1.9	2.8636	14.1672	4.94728	1.36
550	86.3	6.4	7.4	-	-	2.8605	14.211	4.96804	1.45
650	94.3	5.7	-	-	-	2.8608	14.2313	4.97445	1.46
700	100.0	-	-	-	-	2.8634	14.2447	4.97469	1.51
750	100.0	-	-	-	-	2.8621	14.2492	4.97846	1.52
800	100.0	-	-	-	-	2.8612	14.2481	4.97963	1.64
850	100.0	-	-	-	-	2.86308	14.24897	4.97680	2.02

Source: The authors.

The presence of metallic Ni in the pre-calcined sample shows the occurrence of these oxi-reduction reactions. The compounds Co_3O_4 and NiO possibly formed by the decomposition of their carbonates from gel drying and burning that contains citrate and acetate ions, as illustrated in the reactions (BRAUER, 1965), given by equations (6) and (7)

$$6\,CoCO_{3(s)} + O_{2(g)} \xrightarrow{\Delta} 2\,Co_3O_{4(s)} + 6\,CO_{2(g)}, \quad (6)$$

$$NiCO_{3(s)} \xrightarrow{\Delta} NiO_{(s)} + CO_{2(g)}, \quad (7)$$

where Co_3O_4 is a mixed oxide of CO^{2+} and Co^{3+}, so the remaining CO^{2+} must be oxidized by oxygen to be incorporated into the NCM.

Analyzing the phases presented in Table 1 it can be verified that calcined NMC at low temperatures is initially rich in manganese (indicating that NMC rich in Mn can be obtained at low synthesis temperatures) and lithium, which occupies alkaline ion sites between the transition metal layers and is also at the transition metal sites of the *R-3m* structure.

As the temperature rise (T > 700 °C), the remaining nickel and cobalt oxides are incorporated into the lamellar structure, thus forming stoichiometric $Li_xNi_{1/3}Mn_{1/3}Co_{1/3}O_2$. Cao *et al.* (2016) also obtained NMC at 700 °C by the sol-gel method, however with a longer treatment time of 16 hours, thus requiring more energy for the synthesis. Zhang *et al.* (2013) synthesized NMC by a modified sol-gel method using a different chelating agent, however, to obtain crystalline NMC it was necessary to calcine at 850 °C for 5 hours, requiring more energy than the method used in this study.

The $LiNi_{1/3}Mn_{1/3}Co_{1/3}O_2$ compound has α-$NaFeO_2$ type structure, belonging to *R-3m* space group, with hexagonal unit cell. The lattice parameter ratio value, c/a (dimensionless), Table 1, provides information about the hexagonal structure of the compound, while peak separation (006)-(102) and (108)-(110) is a criterion for evaluation of layered structure formation(CAO *et al.*, 2016; CHO *et al.*, 2005; WANG *et al.*, 2022).

Figure 2 shows the peak region (006)-(102) and (108)-(110) of the diffractograms of all synthesized samples, where it was observed that with the increase of the calcination temperature there is an increase in the sharpness of these peaks. This indicates the growth of the NMC layer ordering as well as the increase in its crystallinity. All samples obtained had c/a values, Table 1, greater than 4.90, which is described in the literature as a value indicating a well-ordered hexagonal structure (CAO *et al.*, 2016; CHO *et al.*, 2005).

Figure 2 – Magnification of diffractograms of $LiNi_{1/3}Mn_{1/3}Co_{1/3}O_2$ samples.

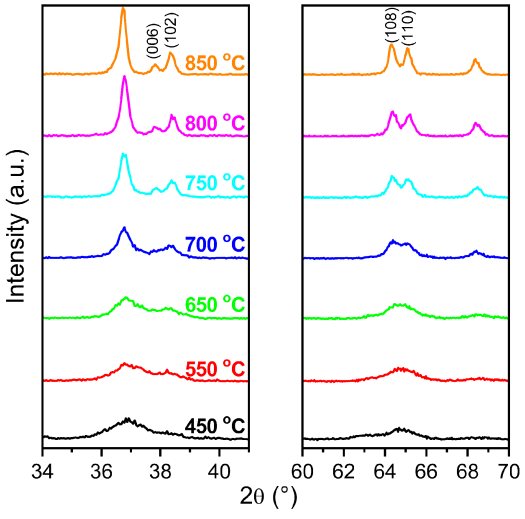

Source: The authors.

In the NMC structure, the oxygen atoms occupy sites 6c, transition metals (manganese, cobalt, and nickel) are isotropically distributed at sites 3b and lithium ions are found at sites 3a. However, a structural disorder may occur due to site exchange between Li^+ and Ni^{2+} ions due to the similarity of ionic radius r_{Li^+} =0.76Å and $r_{Ni^{2+}}$ = 0.69Å and the small energy formation of this defect is calculated as around 0.6 eV (HOANG; JOHANNES, 2016). This cation exchange is undesirable as it decreases the amount of lithium that can be extracted from the material, thereby decreasing charge capacity. This effect can be monitored by ratio between (003) and (104) peak intensity , when the ratio $I_{(003)}/I_{(104)}$ is less than 1.2 it means that there is considerable cation exchange in the material (SHAJU; RAO; CHOWDARI, 2002).

Table 2 shows the peak intensity ratio for each compound. The samples obtained at low temperatures presented the highest cation exchange values, confirming that there is an excess of lithium (or lack of transition metal) that occupies the transition metal sites, as verified in the diffractograms. As the calcination temperature increased, the value of the ratio $I_{(003)}/I_{(104)}$ increased and the amount of lithium in the transition metal layer decreased, indicating less cation position exchange, that is, a growth of the structural order.

Table 2 – Peak intensities ratio of peaks (003) and (104) and amounts of lithium at site 3b obtained by Rietveld refinement.

Temperature (ºC)	$I_{(003)}/I_{(104)}$
450	1.22356
550	1.13359
650	1.38769
700	1.27711
750	1.32915
800	1.42312
850	1.50924

Source: The authors.

To optimize NMC as active material in the lithium-ion battery cathode, micro deformation, which is understood as a percentage of defects in the structure, should be minimized as it makes difficult to lithium ions to diffuse during charging and discharging processes. On the other hand, the size of the crystallite should be maximized, since the larger the crystallite the greater the structural order and consequently fewer the defects are.

In Figure 3 there is a decrease in full width at half maximum (FWHM) and an increase in the absolute intensity of peak (003) proportional to the increase in heat treatment temperature, revealing the growth of the crystallite size.

Figure 3 – Magnification of (003) diffractograms peak for the samples.

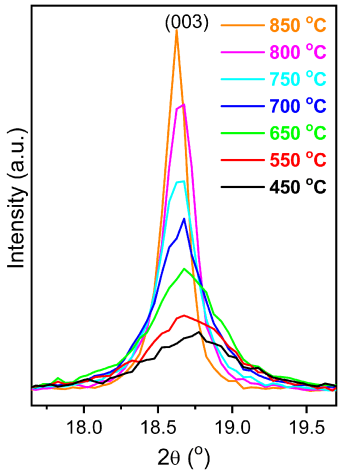

Source: The authors.

Figure 4(a) shows the relationship between crystallite size, obtained by Rietveld refinement, Scherrer and Williamson-Hall methods (BURTON *et al.*, 2009; MANIAMMAL; MADHU; BIJU, 2017), models against calcination temperature. Figure 4(b) shows the microstrain obtained by Rietveld refinement and against calcination temperature. As the temperature rises there is an increase in the size of the crystallite and a decrease in the microstrain. This is due to an increase in the volume of the crystallites reducing the defects between them. In addition, the microstrain values indicate that the samples calcined at temperatures above 700 ºC are very similar in structural ordering.

Scanning electron microscopy

To optimize the electrochemical properties, the electroactive material should have small grains, i.e., a high surface area to facilitate the diffusion of lithium ions and electrolyte wetting. The morphological characteristics of all NMC samples are shown in Figure 5.

The synthesized materials are very homogeneous, porous and have very small particles, useful to obtain ionic intercalation layered compounds with excellent electrochemical properties. Moreover, it was observed that increasing the calcination temperature, occurs a grains dissociation, which promotes a relative increase of the surface area.

Figure 4 – (a) Crystallite size calculated by Rietveld refinement, Scherrer and Williamson-Hall methods and (b) microstrain calculated by Rietveld and Williamson-Hall as a function of $LiNi_{1/3}Mn_{1/3}Co_{1/3}O_2$ calcination temperature.

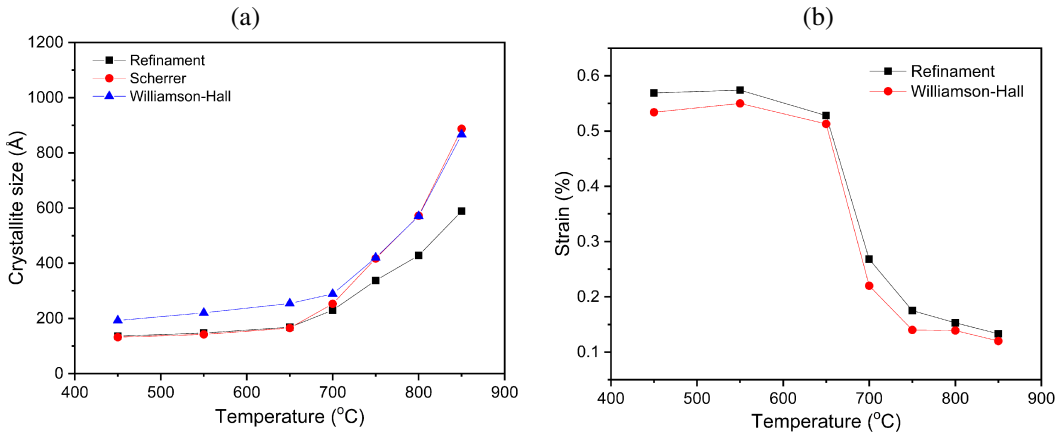

Source: The authors.

Figure 5 – 20.000 × micrographs of $LiNi_{1/3}Mn_{1/3}Co_{1/3}O_2$ samples.

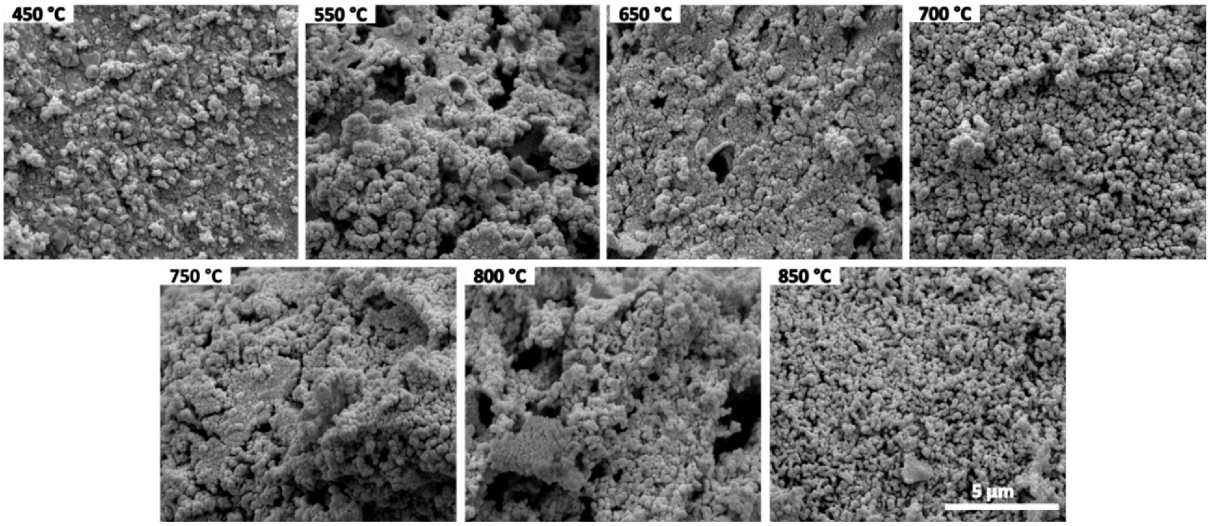

Source: The authors.

FTIR and raman spectroscopy

Figure 6 shows the FTIR and Raman spectra of the NMC samples. $LiNi_{1/3}Mn_{1/3}Co_{1/3}O_2$ belongs to the *R-3m* space group corresponding to the D^5_{3d} spectroscopic space group, which has two active modes in Raman ($A_{1g} + E_g$) and four infrared active modes ($2A_{2u} + 2E_u$) (RILEY *et al.*, 2011).

In the FTIR spectrum, Figure 6(a), there are three NMC bands located at 445, 530 and 591 cm^{-1}, the first and last being due to the O-M-O bond bending vibration and the second to the stretching of the octahedron MO_6 connection. As the calcination temperature increases, there is a reduction in the absorption intensity of the bands around 3400 cm^{-1}, characteristic of the O-H stretch, and 1645 cm^{-1}, which corresponds to the doubling of the H-O-H bond of water molecules, indicating the reducing the content of this compound in the samples with increasing temperature. The bands located at 480, 893, 1100, 1434, and 1490 cm^{-1} are attributed to the vibrations of the CO_3^{2-} ion (LIN *et al.*, 2001). The XRD identified the presence of lithium carbonate only in the pre-calcined sample, Table 1, since this technique detects only carbonate amounts higher than 1%, the FTIR was more sensitive to this specie, identifying its presence in all samples. However, it is clearly noted that the carbonate content decreases with increasing temperature, so that lithium is incorporated into the NMC.

Figure 6 – FTIR spectra (a) complete, (b), (c) and (d) are selected range

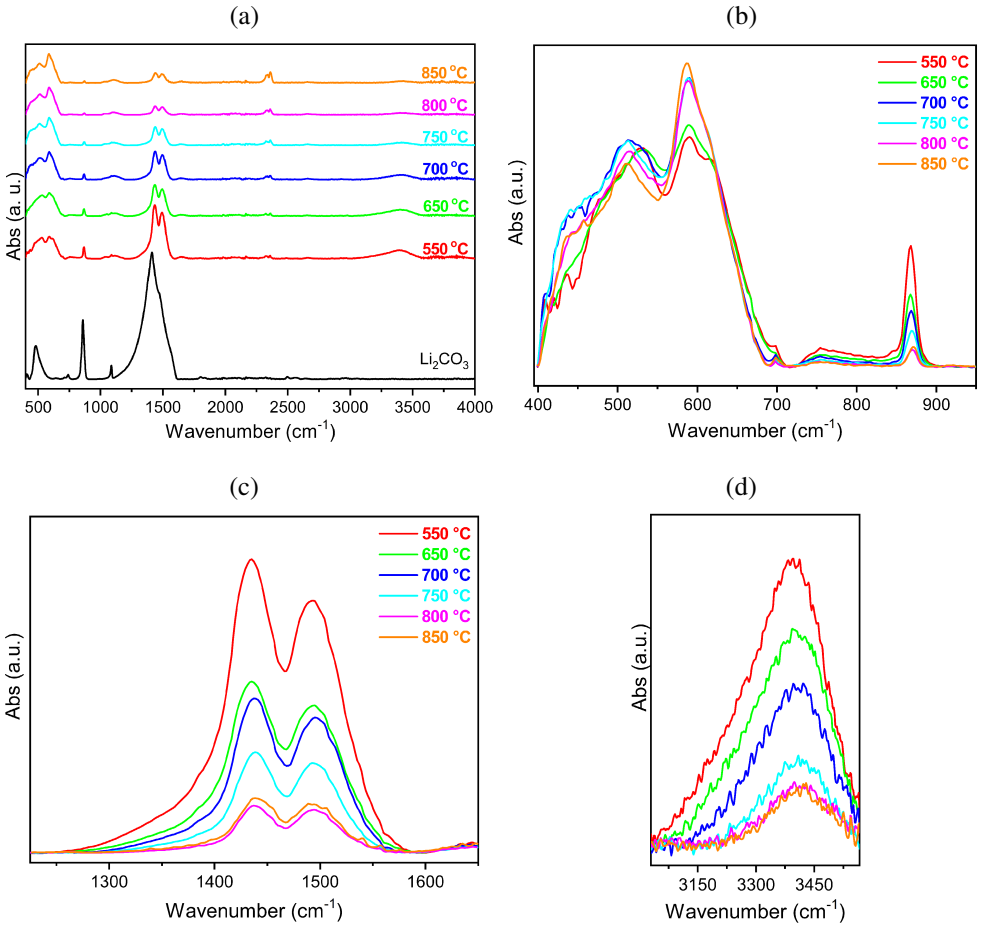

Source: The authors.

Furthermore, it is observed that for calcined samples above 800 °C the bands associated with carbonate, Figure 6(c), and water, Figure 6(d), remain approximately equal, which may be associated with a residual amount of this substance due to the reaction with CO_2 and H_2O present in the air, thus being superficial.

The Co_3O_4, identified by the Rietveld refinement in the 550 °C calcined sample, Table 1, has two bands around 560 and 660 cm^{-1}, corresponding to the M-O bond stretch, and for the first peak M is Co^{3+} coordinated octahedrally and for the second CO^{2+} coordinated tetrahedrally (NASSAR; AHMED, 2011). Figure 6(b) shows a "shoulder" in the specimen of the calcined sample at 550 °C at approximately 620 cm^{-1}, absent in the other samples, associated with the present Co_3O_4. NiO shows a band from the Ni-O bond stretch of approximately 470 cm^{-1}, however, clear observation of this band in the spectrum, Figure 6(b), was not possible due to the proximity to a CO_3^{2-} band at 480 cm^{-1} (KENNDY *et al.*, 2014).

In the Raman spectrum of Figure 7, the 475 cm^{-1} band is assigned to the Eg mode (M-O fold), while the 600 cm^{-1} band to the NMC mode (A_{1g}) (M-O stretch). The broad bands observed in the spectrum suggest a strong structural disorder within the NMC octahedral (MO_6) due to the difference in bond lengths and cation masses of the M-O bonds, as well as the position shift between Li^+ and Ni^{2+} ions (RILEY *et al.*, 2011; LI; WEI; EHRENBERG, 2008). The intensity increases of the bands, when accompanied by their deviation to the red region, is related to the structural disorder increasing. However, in Figure 7 there is no band shift, so the variation in peak intensity may have been caused by the focus of the sample and the large relative size of the point (RILEY *et al.*, 2011).

Electrochemical property

To compare the effect of the calcination temperature on the electrochemical activity of the NCM regarding the mobility of lithium ions, deinterleaving them from the crystalline structure in the electrochemical charge processes and reversibly intercalating them in the structure in the discharge processes, electrodes from the calcined samples were prepared. at 700 and 850 °C, which do not have contaminating phases.

Figure 7 – Raman spectra of $LiNi_{1/3}Mn_{1/3}Co_{1/3}O_2$ samples.

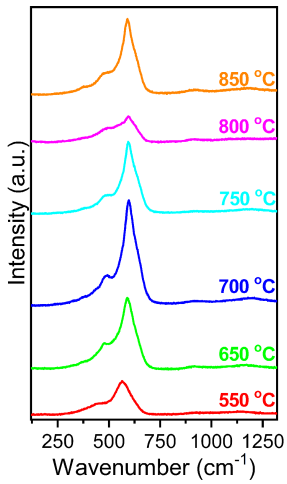

Source: The authors.

Figure 8 shows the variation in discharge capacity at 0.1C between 3.00 and 4.70 V vs. Li/Li^+. The observed capacities were 174.0 mA h g^{-1} for the sample at 700 ºC and 170.0 mA h g^{-1} for 850 ºC, a value close to the literature for NMC (CAO *et al.*, 2016).

Figure 8 – Discharge capacity at 0.1C in the potential range from 3.00 to 4.70 V vs. Li/Li^+ of $LiNi_{1/3}Mn_{1/3}Co_{1/3}O_2$ samples calcined at 700 and 850 ºC.

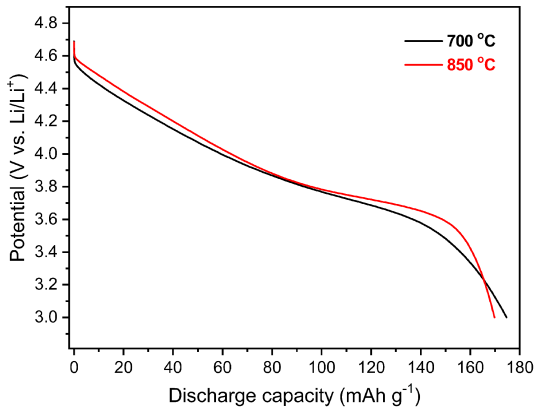

Source: The authors.

In an attempt to increase the discharge capacity of the NMC, the window of applied potential was varied, as shown in Figure 9.

It is observed, in Figure 9, that with the increase of the cutting potential there is an increase of the discharge capacity for both samples, and the calcined sample in 850 ºC presented higher initial discharge capacities in each interval, however, presented lower retention than the calcined sample at 700 ºC.

Figure 9 – Effect of the gradual increase of the potential on the 0.2C discharge capacity of the calcined 700 and 850 ºC $LiNi_{1/3}Mn_{1/3}Co_{1/3}O_2$ sample.

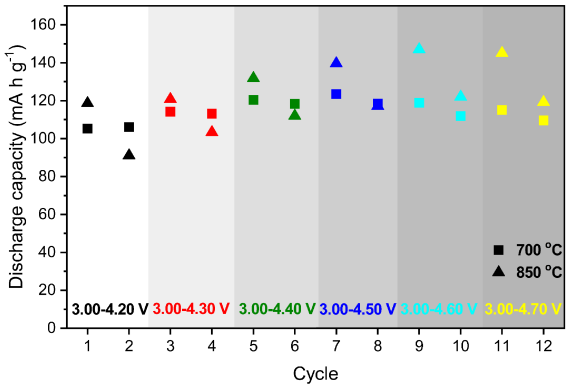

Source: The authors.

Figure 10 shows the retention of the discharge capacities of the calcined samples at 700 and 850 °C for 10 cycles at 0.2C, where it can be seen that the calcined sample at the highest temperature had a slightly higher retention capacity with an increasing number of cycles, due to its higher structural ordering.

Figure 10 – Discharge capacity in the range of 3.00 to 4.70 V at 0.2C, depending on the number of cycles of the $LiNi_{1/3}Mn_{1/3}Co_{1/3}O_2$ samples calcined at 700 and 850 ºC.

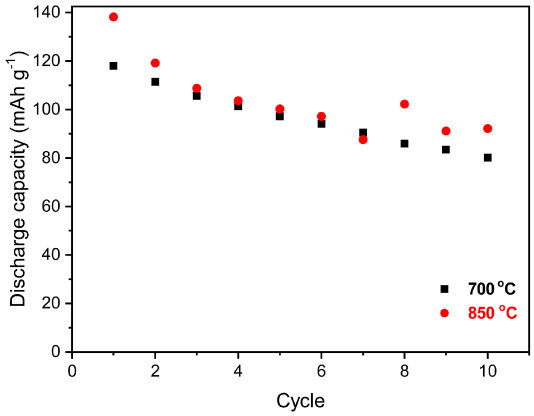

Source: The authors.

Conclusion

In this study, the $LiNi_{1/3}Mn_{1/3}Co_{1/3}O_2$ was successfully synthesized by the modified sol-gel method even under low pre-calcination heating rates. Non-stoichiometric NMC formation was observed at low calcination temperatures (450, 550 and 650 ºC) and stoichiometric NMC from 700 °C with treatment time of only 1 hour, showing that the synthetic route used is convenient for industrial application, as it does not require high temperatures to obtain

the desired compound, reducing cathode manufacturing costs.

In addition, X-ray diffraction showed that the cation exchange between nickel and lithium ions decreases with increasing calcination temperature, indicating that this phenomenon can be controlled during powder synthesis.

Acknowledgments

Authors are thankful to the Laboratório de Microscopia Eletrônica e Microanálise - LMEM/UEL, Laboratório de Difração de Raios X – LARX/LDRX/UEL and to the financial support of CNPq.

References

BORCHERT, H.; SHEVCHENKO, E. V., ROBERT, A.; MEKIS, I.; KORNOWSKI, A.; GRÜBEL, G.; WELLER, H. Determination of nanocrystal sizes: a comparison of TEM, SAXS, and XRD studies of highly monodisperse CoPt3 particles. *Langmuir*, Washington, v. 21, n. 5, p. 1931-1936, 2005.

BRAUER, G. *Handbook of preparative inorganic chemistry*. 2nd ed. New York: Academic Press, 1965.

BURTON, A. W.; ONG, K.; REA, T.; CHAN, I. Y. On the estimation of average crystallite size of zeolites from the Scherrer equation: a critical evaluation of its application to zeolites with one-dimensional pore systems. *Microporous and Mesoporous Materials*, Amsterdam, v. 117, n. 1/2, p. 75-90, 2009. DOI: https://doi.org/10.1016/j.micromeso.2008.06.010.

CAO, X. *et al.* Synthesis and characterization of $Lini_{1/3}CO_{1/3}MN_{1/3}O_2$ as cathode materials for li-ion batteries via an efficacious sol- gel method. *Int. J. Electrochem* Sci., Bor, v. 11, p. 5267–5278, 2016. DOI: 10.20964/2016.06.93

CHO, T. H.; PARK, S. M.; YOSHIO, M.; HIRAI, T.; HIDESHIMA, Y. Effect of synthesis condition on the structural and electrochemical properties of $Li[Ni_{1/3}Mn_{1/3}Co_{1/3}]O_2$ prepared by carbonate co-precipitation method. *Journal of Power Sources*, Lausanne, v. 142, n. 1/2, p. 306–312, 2005. DOI: https://doi.org/10.1016/j.jpowsour.2004.10.016.

GONÇALVES, N. S. *et al*. Size–strain study of NiO nanoparticles by X-ray powder diffraction line broadening. *Materials letters*, Amsterdam, v. 72, p. 36-38, 2012.

HOANG, K.; JOHANNES, M. Defect physics and chemistry in layered mixed transition metal oxide cathode materials: (NI,CO,MN) VS (NI,CO,AL). *Chemistry of Materials*, Washington, v. 28, n. 5, p. 1325–1334, 2016. DOI: https://doi.org/10.1021/acs.chemmater.5b04219.

JAMIL, S.; WANG, G.; FASEHULLAH, M.; MAOWEN, X. Challenges and prospects of nickel-rich layered oxide cathode material. *Journal of Alloys and Compounds*, Amsterdam, V. 909, n. 15, p. 1–28, 2022. DOI: https://doi.org/10.1016/j.jallcom.2022.164727.

KENNEDY, L. J.; MAGESAN, P.; VIJAYA, J. J.; UMAPATHY, M. J.; ARULDOSS, U. Biominerals doped nanocrystalline nickel oxide as efficient humidity sensor: a green approach mater. *Mater Sci Eng B Solid State Mater Adv Technol.*, Lausanne, v. 190, p. 13–20, 2014.

KIZILTAŞ-YAVUZ, N.; HERKLOTZ, M.; HASHEM, A. M.; ABUZEID, H. A.; SCHWARZ, B.; EHRENBERG, H.; MAUGER, A.; JULIEN, C. M. Synthesis, structural, magnetic and electrochemical properties of $LINI_{1/3}CO_{1/3}MN_{1/3}O_2$ prepared by a sol–gel method using table sugar as chelating agent. *Electrochimica acta*, Oxford, v. 113, p. 313–321, 2013. DOI: https://doi.org/10.1016/j.electacta.2013.09.065

LI, X.; WEI, Y. J.; EHRENBERG, H. Characterizations on the structural and electrochemical properties of $LINI_{1/3}CO_{1/3}MN_{1/3}O_2$ prepared by a wet-chemical process. *Solid State Ionics*. Amsterdam, v. 178, n. 39/40, p. 1969–1974, 2008.

LIN, S. P.; FUNG, K. Z.; HON, Y. M.; HON, M. H. Crystallization mechanism of linio 2 synthesized by pechini method. *Journal of Crystal Growth*, Amsterdam, v. 226, p. 148–157, 2001. DOI: https://doi.org/10.1016/S0022-0248(01)01363-X.

NASSAR, M. Y.; AHMED, I. S. Hydrothermal synthesis of cobalt carbonates using different counter ions: an efficient precursor to nano-sized cobalt oxide (CO_3O_4). *Polyhedron*, London, v. 30, n. 15, p. 2431–2437, 2011. DOI: https://doi.org/10.1016/j.poly.2011.05.039.

MANIAMMAL, K.; MADHU, G.; BIJU, V. X-ray diffraction line profile analysis of nanostructured nickel oxide: shape factor and convolution of crystallite size and microstrain contributions. *Physica E: Low-dimensional Systems and Nanostructures*, Amsterdam, v. 85, p. 214-222, 2017. DOI: https://doi.org/10.1016/j.physe.2016.08.035

OHZUKU, T.; MAKIMURA, Y. Layered lithium insertion material of Lico $_{1/3}CO_{1/3}MN_{1/3}O_2$ for lithium-ion batteries. *Chem. Lett.*, Tokyo, v. 30, n. 7, p. 642–643, 2001.

RILEY, L. A. et al. Electrochemical effects of ald surface modification on combustion synthesized $LINI_{1/3}CO_{1/3}MN_{1/3}O_2$ as a layered-cathode material. *Journal of Power Sources*, Lausanne, v. 196, n. 6, p. 3317–3324, 2011.

SATHIYA, M.; PRAKASH, A. S.; RAMESHA, K.; SHUKLA, A. K. Rapid synthetic routes to prepare $LINI_{1/3}CO_{1/3}MN_{1/3}O_2$ as a high voltage, high-capacity li-ion battery cathode material. Mater. Res. *Bull.*, New York, v. 44, n. 10, p. 1990–1994, 2009. DOI: 10.1016/j.materresbull.2009.06.007.

SHAJU, K. M.; RAO, G. V. S.; CHOWDARI, B. V. R. Performance of layered LI (NI $_{1/3}CO_{1/3}MN_{1/3}O_2$) as cathode for li-ion batteries. *Electrochimica acta*, Oxford, v. 48, p. 145–151, 2002.

VAALMA, C.; BUCHHOLZ, D.; WEIL, M.; PASSERINI, S. A cost and resource analysis of sodium-ion batteries. *Nature Reviews Materials*, London, v. 3, n. 4, p.1-11, 2018.

WANG, X.; ZHOU, H.; CHEN, Z.; MENG, X. Synchrotron-based X-ray diffraction and absorption spectroscopy studies on layered $LiNi_xMn_yCo_zO_2$ cathode materials: a review. *Energy Storage Materials*, Amsterdam, v. 49, p. 181–208, 2022. DOI: https://doi.org/10.1016/j.ensm.2022.04.012.

ZHANG, Y.; WU, X.; LIN, Y.; WANG, D.; ZHANG, C.; HE, D. Synthesis of $LINI_{1/3}CO_{1/3}MN_{1/3}O_2$ cathode material by a modified sol–gel method for lithium-ion battery. *Journal of Sol-Gel Science and Technology*, Boston, v. 68, n. 2, p. 169–174, 2013. DOI: 10.1007/s10971-013-3148-9.

Received: Fev. 24, 2022
Accepted: May 03, 2022
Published: May 15, 2022